

# Pattern Formation in Populations with Density-Dependent Movement and Two Interaction Scales

Ricardo Martínez-García<sup>1,2,\*</sup>, Clara Murgui<sup>1</sup>, Emilio Hernández-García<sup>1</sup>, Cristóbal López<sup>1</sup>,

**1 IFISC (Instituto de Física Interdisciplinar y Sistemas Complejos), CSIC-UIB, Campus UIB, Palma de Mallorca, Spain.**

**2 Department of Ecology and Evolutionary Biology, Princeton University, Princeton NJ, 08544-1003, USA.**

\* ricardom@princeton.edu

## Abstract

We study the spatial patterns formed by a system of interacting particles where the mobility of any individual is determined by the population crowding at two different spatial scales. In this way we model the behavior of some biological organisms (like mussels) that tend to cluster at short ranges as a defensive strategy, and strongly disperse if there is a high population pressure at large ranges for optimizing foraging. We perform stochastic simulations of a particle-level model of the system, and derive and analyze a continuous density description (a nonlinear diffusion equation). In both cases we show that this interplay of scale-dependent-behaviors gives rise to a rich formation of spatial patterns ranging from labyrinths to periodic cluster arrangements. In most cases these clusters have the very peculiar appearance of ring-like structures, i.e., organisms arranging in the perimeter of the clusters, that we discuss in detail.

## Introduction

Individual based models are of great relevance in many disciplines, ranging from condensed matter [1] to biology [2, 3], economics and social dynamics [4]. They allow to simulate some simple dynamical rules and study its consequences at a global population scale. In an ecological context individual based models are commonly used to investigate collective behavior and the emergence of patterns, which are central issues in theoretical ecology [5].

In this paper, we propose a model to study the formation of spatial patterns in a population of organisms in which interactions affect their mobility. We assume that, during the time scales of interest here, no other dynamical processes such as birth, reproduction and death occur. The movement of any individual depends on the distribution of its conspecifics at two length scales. We thus focus on the problem of group formation and spatial aggregation [6–8] although this approach may be used in the more general context of collective movement [9] including birds flocks [10, 11], fish swarms [12, 13], and mammals herds [14], and also to address the effect of spatial degrees of freedom in evolutionary problems [15].

Spatial aggregation is a widespread phenomenon in living systems, resulting from the combination of individual movement with interspecific and intraspecific interactions [3, 16]. Therefore, a mathematical description of group formation should include all these mechanisms, and several ways of integrating collective interactions with individual movement have been proposed [2, 9, 17–20]. A very important type of models considers that interactions influence only the movement of the individuals disregarding any other intra- and inter-specific interactions. They are relevant to study

animal or organism dispersal wherever there is an increase of the diffusivity with the local density because of population pressure [2, 3]. Extensions of these works also account for the effect of conspecifics located at separated positions [2, 17, 21], including nonlocal spatial interactions. This family of models results in nonlocal nonlinear diffusion equations [22, 23] for the population density. From a biological point of view, they usually account for a single class of interactions, and diffusivity depends on the population density over one neighborhood of the focal individual. However, in a more general framework, many different interactions of diverse nature are relevant within a population, so these single-scale approaches might not describe the complete set of processes taking place. For instance, high long-range densities (i.e. densities of others within a long distance around a focal one) may encourage animal mobility due to intraspecific competition for resources, while on a shorter spatial scale individuals may arrange in cooperative aggregations so that the predation risk decreases. Also in the decision-making process that underlies collective movement, animals choose how to move depending on their neighbors at different distances, so they guarantee the cohesion of the group [10, 24, 25]. In a rather different context, the formation of patterns of vegetation has been also traditionally thought to be a consequence of the interplay between plant interactions at two different scales: short-range facilitation and long-range competition [26–30], although this has been a contentious claim [31]).

Mussel beds are one of the paradigmatic examples of spatial aggregation in nature. Both theoretical [32, 33] and experimental [34, 35] studies have showed that interactions among individuals modify only their diffusion coefficient. Mussels movement is encouraged when their density is large in a long-range, since the competition for algae prevents the formation of big clumps. However, on a shorter spatial scale, they arrange in cooperative aggregations so that wave stress and predation risk diminish. Within this framework, we present a model of interacting particles where the mobility of the individuals, i.e. its diffusivity, depends on two spatial scales. Movement is encouraged when the density is high in a long-range (competition), and inhibited if it is so in a short-range (i.e., cooperative aggregations are favored at shorter scales). Although motivated by previous works [32–37], our approach differs from these studies in considering only individual dispersal and not interactions with the environment and other species to explain spatial aggregation. In addition, the Lévy flight characteristic of the motion, which is central in those studies, is disregarded in our analysis.

In the following sections pattern formation will be studied combining numerical and analytical techniques both in the discrete-particle dynamics and its continuous-field density equation.

## Materials and Methods

### Individual-based dynamics

Let us consider a population of  $N$  individuals undergoing Brownian movement with a diffusion coefficient that depends on the densities of conspecifics at two separated length-scales: a mean density  $\tilde{\rho}_s$  at short range,  $R_s$ , and a mean density  $\tilde{\rho}_l$  over a long one,  $R_l$  ( $R_s < R_l$ ). We will denote the position of each particle by  $\mathbf{r}_i = (x_i, y_i)$  at any time  $t$  in a two-dimensional square system of lateral extent  $L$  with periodic boundary conditions.

The dynamics of each particle  $i = 1, \dots, N$  is then given by

$$\dot{\mathbf{r}}_i = \sqrt{2D(\mathbf{r}_i, \tilde{\rho}_s, \tilde{\rho}_l)} \boldsymbol{\eta}_i(t), \quad (1)$$

where the diffusivity  $D$  is, in general, a positive continuous function of  $\tilde{\rho}_l$  and  $\tilde{\rho}_s$ .  $\boldsymbol{\eta}_i(t)$  is a white Gaussian vector noise with zero mean and with time-correlation matrix given by  $\langle \boldsymbol{\eta}_i(t) \boldsymbol{\eta}_j(t') \rangle = \mathbf{1} \delta_{ij} \delta(t - t')$ .  $\mathbf{1}$  is the identity matrix. Eq. (1) should be interpreted within the Itô calculus, since the stop/movement behavior is assumed to occur at the beginning of each time step [22]. The mean densities are defined as:

$$\tilde{\rho}_\mu(\mathbf{r}) = \frac{N_\mu}{\pi R_\mu^2}, \quad (2)$$

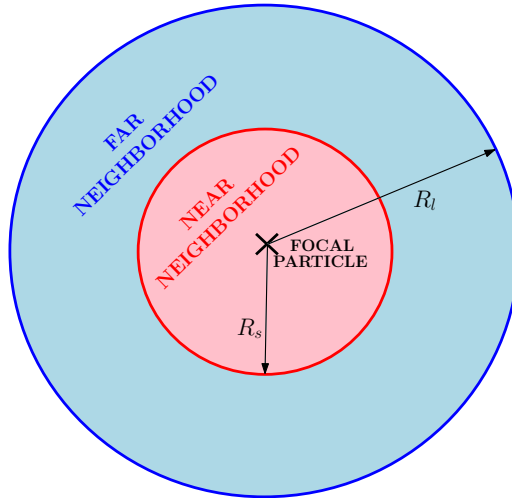


**Figure 1. Interaction neighborhoods.** Short- and long-range interaction neighborhoods for a given individual. The regions are defined by their radius  $R_s$  and  $R_l$  respectively.

with  $\mu \equiv s, l$ .  $N_s$  and  $N_l$  are the number of individuals found in a near and far neighborhood of the particle at  $\mathbf{r}$ , respectively (see Fig. 1). Note that, since the number of individuals does not change, the global density  $\rho_0 = N/L^2$  remains constant in time.

The main focus of this approach is on species that switch between the tendency to aggregation and to dispersion as the number of surrounding individuals increases at different length scales. In particular, we address the case of competitive long range interactions and facilitation at a shorter scale. This is the observed framework in mussel beds, where patterns appear due to the interaction between two opposing mechanisms: competition for resources at a large scale and defense against predators and waves stress at shorter distance [32, 33, 35]

To model this behavior we consider that the diffusivity,  $D$ , is enhanced with increasing the long-range density, and reduced with increasing short-range density. This can be written as  $D = D_0 g(a - b\tilde{\rho}_s + c\tilde{\rho}_l)$  if  $g$  is an arbitrary function with positive derivative,  $\partial_x g(x) > 0$ .  $D_0$  is a constant diffusivity and  $a$ ,  $b$ , and  $c$  are positive parameters. Note that with the expression  $a - b\tilde{\rho}_s + c\tilde{\rho}_l$  we indicate, as mentioned before, that the *tendency* of a particle to move decreases with the short-range mean density ( $-b\tilde{\rho}_s$ ) and increases with the long-range one ( $c\tilde{\rho}_l$ ). The function  $g$  takes its maximum (minimum) value in the limit  $\tilde{\rho}_l \gg \tilde{\rho}_s$  ( $\tilde{\rho}_s \gg \tilde{\rho}_l$ ). For simplicity we restrict to the case  $0 \leq g \leq 1$  so the diffusivity of the particles varies between 0 and  $D_0$ .  $D_0$  is the diffusion coefficient of the population when movement is extremely promoted ( $\tilde{\rho}_l \gg \tilde{\rho}_s$ ).

With the above mentioned properties of  $g$  we choose as an example (the main results are independent of the particular  $g$ )

$$g(\mathbf{r}_i(t)) = \frac{1 + \tanh [2(a - b\tilde{\rho}_s(\mathbf{r}_i) + c\tilde{\rho}_l(\mathbf{r}_i)) - 1]}{2}, \quad (3)$$

where parameters  $b$  and  $c$  weight the importance of the short and the long-range densities, respectively, and parameter  $a$  gives the diffusivity of an individual when short and long-range densities are equal and have the same weight. Notice once again that  $g \rightarrow 0$  if  $\tilde{\rho}_s \gg \tilde{\rho}_l$  and  $g \rightarrow 1$  if  $\tilde{\rho}_l \gg \tilde{\rho}_s$ .

## Continuum description

The particle dynamics given by Eq. (1) allows an intensive numerical exploration. To complement the study and obtain analytical results it is essential to have a simplified continuum equation of the model, where the population is described in terms of a collective variable: the local density of individuals  $\rho(\mathbf{r})$ . This equation can be derived following Dean's approach [38] from the stochastic

particle dynamics presented in the previous section, which uses Itô calculus. Considering a mean-field approximation (i.e., neglecting fluctuations in the density) we obtain for the mean particle density

$$\frac{\partial \rho(\mathbf{r}, t)}{\partial t} = D_0 \nabla^2 [g(\tilde{\rho}_s, \tilde{\rho}_l) \rho(\mathbf{r}, t)], \quad (4)$$

where the mean long- and short-range densities are computed as

$$\tilde{\rho}_\mu(\mathbf{r}, t) = \int G_\mu(\mathbf{r} - \mathbf{r}') \rho(\mathbf{r}', t) d\mathbf{r}', \quad (5)$$

where  $G_\mu$ , with  $\mu \equiv s$  or  $\mu \equiv l$ , are the short and long range kernel functions that define both interaction scales. The kernel functions are normalized and have units of inverse of area

$$G_\mu(|\mathbf{r}|) = \begin{cases} \frac{1}{\pi R_\mu^2} & \text{if } |\mathbf{r}| \leq R_\mu \\ 0 & \text{if } |\mathbf{r}| > R_\mu, \end{cases} \quad (6)$$

$R_\mu$  ( $\mu \equiv s, l$ ) define, as in the individual based approach, the short and long interaction ranges, respectively.

## Results

A direct exploration of pattern formation in the model starts from Monte Carlo numerical simulations of the individual-based dynamics given by Eq. 1. To unveil the relationships between the two spatial scales that promote the formation of spatial structures, we isolate in our analysis the relative importance of the short and long-range densities fixing all the parameters of the model ( $R_s$ ,  $R_l$ ,  $D_0$ ,  $N$ ,  $a$ ; see caption of Fig. 2 for details), except  $b$  and  $c$ , that weight the influence of  $\tilde{\rho}_s$  and  $\tilde{\rho}_l$  on the diffusivity.

Depending on the relationships between this pair of parameters the population may show a homogeneous distribution (Fig. 2, top panel) or arrange developing spatial aggregations (bottom panels of Fig. 2). Two classes of patterns are observed: labyrinth distributions and isolated spots [33, 34] arranged in a hexagonal matrix. A relevant and singular feature is the shape of the aggregations, with most of the individuals clumped in the borders of the cluster and an almost empty inner area. Similar ring-like structures have been previously reported in plant ecology and studied with models based on mechanisms very different from ours, but that share with our approach the presence of competitive and facilitative interactions [39, 40].

A deeper understanding of the pattern formation dynamics can be addressed using the continuum description given by Eq. (4). To corroborate the correspondence between the individual based description by Eq. (1) and the continuous approach in terms of Eq. (4), we numerically integrate Eq. (4). Kernels are fixed as given by Eq. (6) and the parameters take the same values as in Fig. 2 to allow a direct comparison with the discrete simulations (see caption of Fig. 3 for details). The labyrinth and spot patterns showed in Fig. 3 exhibit a good agreement with the distributions of Fig. 2 resulting from the stochastic particle dynamics. In particular, details of hollow clusters for both micro and macro descriptions are plotted in Fig. 4. The distribution of the particles within the clusters is a particularly interesting question that will be discussed later in this section.

We continue with the analytical approach performing a linear stability analysis of Eq. (4). We note that the homogeneous distribution of the  $N$  individuals in the box of size  $L$ , i.e.  $\rho(\mathbf{r}, t) = \rho_0 = N/L^2$  always provides a stationary solution to such equation. The stability of this homogeneous distribution is checked by adding a small perturbation to it, so that  $\rho(\mathbf{r}, t) = \rho_0 + \epsilon \psi(\mathbf{r}, t)$  ( $\epsilon \ll 1$ ). Inserting this into Eq. (4) we find that the perturbation growth rate of  $\psi \propto \exp(\mathbf{k} \cdot \mathbf{r} + \lambda t)$  is given by

$$\lambda(\mathbf{k}) = -\frac{D_0}{2} \left( 1 + \tanh \gamma + \frac{2c\rho_0 \hat{G}_l(\mathbf{k}) - 2b\rho_0 \hat{G}_s(\mathbf{k})}{\cosh^2 \gamma} \right) \mathbf{k}^2, \quad (7)$$

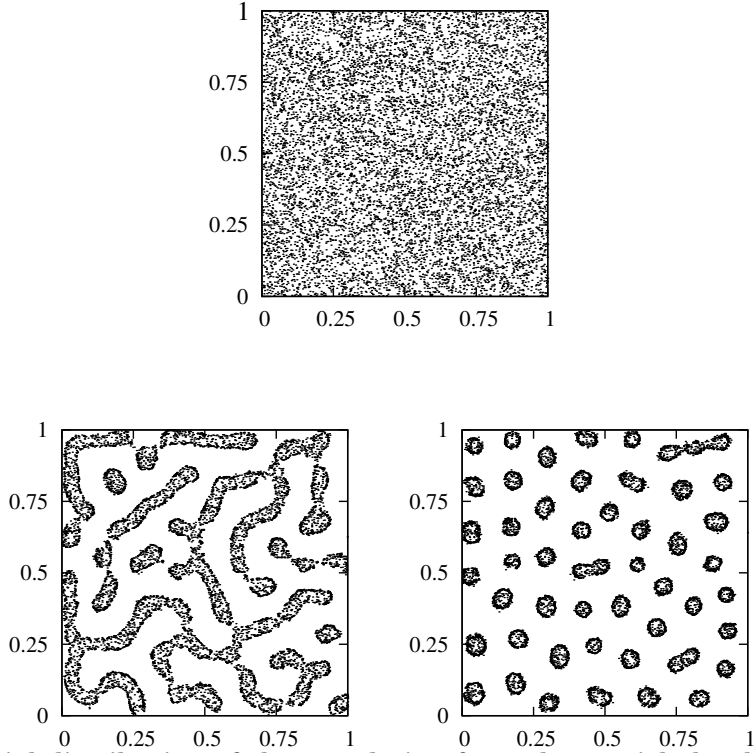


**Figure 2. Spatial distribution of the population from the particle-level model.** Spatial distribution at long times of a population of  $10^4$  individuals using the dynamics of Eq. (1) with a short interaction range  $R_s = 0.05$  and a long interaction length  $R_l = 0.1$ .  $D_0 = 10^{-4}$ ,  $a = 1$  in all the panels. The system is a square area of lateral size  $L = 1$  with periodic boundary conditions. Upper panel:  $b = 3.5 \times 10^{-4}$ ,  $c = 7.0 \times 10^{-4}$  (homogeneous distribution). Left bottom panel:  $b = 8.5 \times 10^{-4}$ ,  $c = 7 \times 10^{-4}$  (labyrinth pattern). Right bottom panel:  $b = 4.3 \times 10^{-4}$ ,  $c = 3.9 \times 10^{-4}$  (spot pattern). Note the rings with higher density in the border.

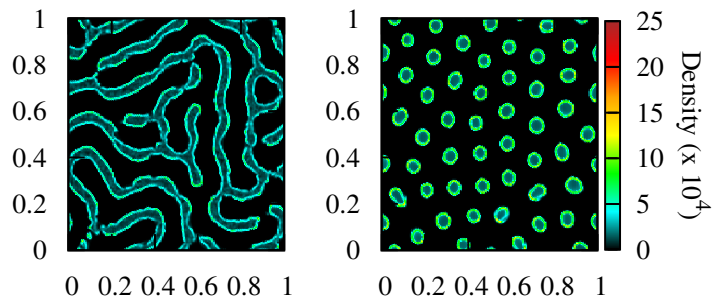


**Figure 3. Solutions of the continuous density equation.** Long time solution of Eq. (4) with a short interaction range  $R_s = 0.05$  and a long interaction length  $R_l = 0.1$ .  $D_0 = 10^{-4}$ ,  $a = 1$  and density  $\rho_0 = 10^4$  in all the panels. An Euler algorithm was implemented and integration performed over a square area with lateral size  $L = 1$  and periodic boundary conditions. Left panel:  $b = 8.5 \times 10^{-4}$ ,  $c = 7 \times 10^{-4}$  (labyrinth pattern). Right panel:  $b = 4.3 \times 10^{-4}$ ,  $c = 3.9 \times 10^{-4}$  (spot pattern).

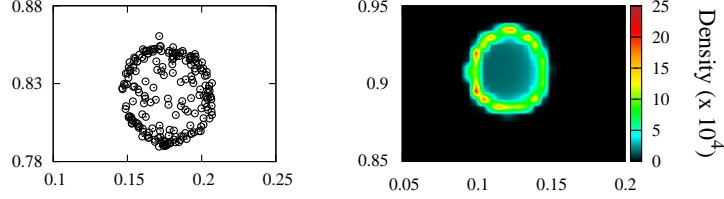


**Figure 4. Comparison of a single ring-like structure in both approaches.** Detailed distribution of the individuals within one of the groups of the spotted pattern in the discrete model (Left) and of the density in one of the patches in the solution of the continuous equation (Right). Parameters:  $b = 4.3 \times 10^{-4}$ ,  $c = 3.9 \times 10^{-4}$ ,  $D_0 = 10^{-4}$ ,  $a = 1$ ,  $R_l = 0.1$  and  $R_s = 0.05$  in all the panels.

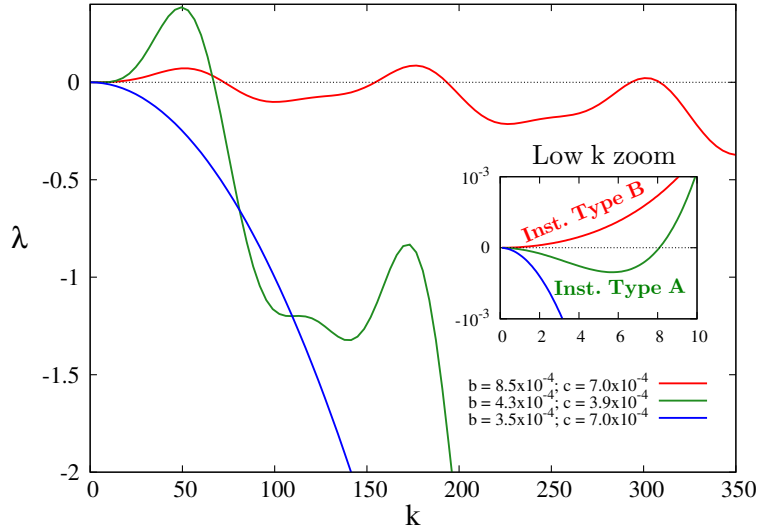


**Figure 5. Perturbation growth rate.** Perturbation growth rate as a function of the wavenumber, Eq. (8), for different values of the parameters  $b$  and  $c$ .  $R_s = 0.05$ ,  $R_l = 0.1$ ,  $D_0 = 10^{-4}$  and  $a = 1$ .

where  $\gamma = 2(a - b\rho_0 + c\rho_0) - 1$ .  $\hat{G}_s(\mathbf{k})$  and  $\hat{G}_l(\mathbf{k})$  are the Fourier transforms of the short-range and the long-range kernels, respectively. Given the choice made for the kernels (Eq. (6)), the Fourier transforms are

$$\hat{G}_\mu(\mathbf{k}) = 2 \frac{J_1(\mathbf{k}R_\mu)}{|\mathbf{k}|R_\mu}, \quad (8)$$

where  $\mu = s$  or  $\mu = l$ , and  $J_1$  is the first order Bessel function. The homogeneous distribution is unstable and then patterns would appear if the maximum of the growth rate (i.e., of the most unstable mode),  $\lambda(\mathbf{k}_c)$ , is positive, which means that the perturbation of periodicity  $2\pi/|\mathbf{k}_c|$  grows with time.  $\lambda$  is showed for different values of the parameters  $b$  and  $c$  in Fig. 5. Depending on the value of  $b$  and  $c$  the model shows two different types of instabilities. Instability A has stable low wavenumbers (green curve in Fig. 5, see inset) that prevent the clusters to grow. The characteristic wavelength of the pattern is well defined around  $k_c = 49.52$ . On the other hand an instability of type B has a band of unstable modes starting at  $k = 0$ , which could allow the clusters to experience some coarsening in time. We observe that labyrinthic structures are formed by this type B instability.

Evaluating the perturbation growth rate in Eq. (7) with Eq. (8), we may compute the phase diagram of the model (see Fig. 6) for parameters  $b$  and  $c$  that gives information about the final spatial distribution of the system, homogeneous or patterned. The reduction of the diffusivity at high short-range densities is the responsible of the formation of patterns since clusters appear when

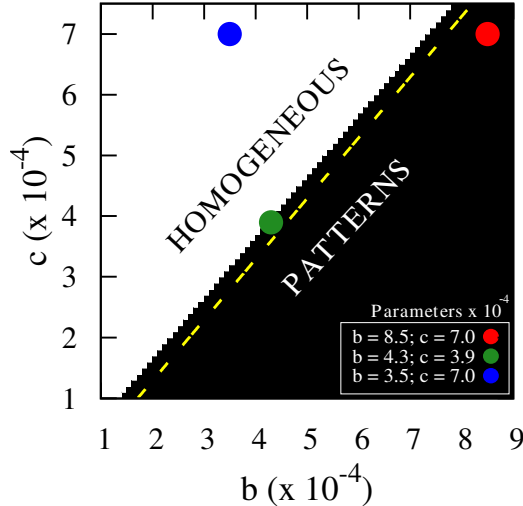


**Figure 6. Phase diagram of the continuous approach.** Parameter space of the continuous model where the regions of patterns and homogeneous solutions have been identified using the perturbation growth.  $R_s = 0.05$ ,  $R_l = 0.1$ ,  $D_0 = 10^{-4}$  and  $a = 1$ . The yellow dashed line shows the transition from Instability A (above the line) to Instability B (below the line).

$b > c$ , that is when  $\rho_s$  is more relevant for the dynamics than  $\rho_l$ . On the other hand, considering the effect of the long-range density alone on the diffusivity, the system shows homogenous distributions regardless of the value of  $c$  when  $b = 0$ . These are expected results since high values of the short-range density reduce the mobility of the individuals promoting clustering, while high values of the long-range density enhance longer displacements in the population, thus leading to homogenous distributions. However, the instability caused by a diffusivity reduction is enhanced by the presence of the  $\rho_l$  dependence because animals in-between two aggregations make longer displacements that allow them to reach a group. A similar argument has been used to explain the formation of clusters of species [41] and vegetation [42] in systems that only present long-range competitive interactions.

In addition, the boundary between both types of instabilities (A for hexagonal clusters, and B for labyrinthic patterns) is given by a change in the sign of the second derivative of the perturbation growth rate at  $k = 0$ . It is represented in Fig. 6 by the yellow dashed line resulting from numerically evaluating

$$\lambda''(k)|_{k=0} = \frac{-D_0}{2} \left( 1 + \frac{2(c-b)}{\cosh^2 \gamma} + \tanh \gamma \right) = 0. \quad (9)$$

The typical scale of the pattern, that is, the distance between aggregates, can be studied with the structure function (Fig. 7). It can be computed for both the patterns of particles and the density distribution. In the first case it is  $S_d(\mathbf{k}) = \left\langle \left| \frac{1}{N} \sum_{j=1}^N e^{i\mathbf{k}\cdot\mathbf{r}_j} \right|^2 \right\rangle$ , where  $\mathbf{r}_j$  is the position vector of particle  $j$ ,  $\mathbf{k}$  is a two-dimensional wave vector with modulus  $k$ , and the average indicates a spherical average over the wave vectors with modulus  $k$  and in time. In the continuous approach, the structure function is calculated as the modulus of the spatial Fourier transform of density field, averaged spherically and in time. Note that both quantities are related but not identical, and their first maximum,  $k_c$ , allows to compute the typical distance between clusters  $d = 2\pi/k_c$ . For the spotted patterns  $k_c = 50.24$  (discrete) and  $k_c = 49.52$  (continuum) so that  $d \approx 0.125 - 0.126$ . Regarding the case of the labyrinth pattern (central panel of Figs. 2 and 3),  $k_c = 56.52$  (discrete) and  $k_c = 51.31$  (continuum), so that the typical distance between aggregates is  $d \approx 0.11$ .

As it was stated before, the ring-like shape of the clusters deserves further consideration. To go deeper into this question we use the one-dimensional version of the model starting from an initial condition consisting of a single pulse of height unity (top panel of Fig. 8). The mean nonlocal densities  $\tilde{\rho}_s$  (dashed red line) and  $\tilde{\rho}_l$  (dashed green line) can be easily obtained and lead to a

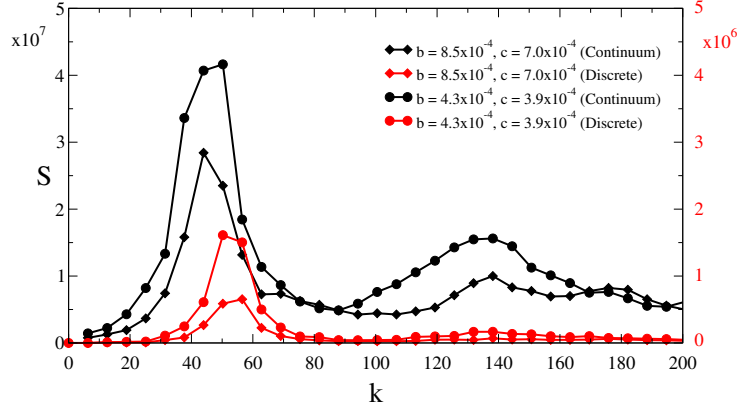


**Figure 7. Structure functions.** Structure function of the patterns obtained with the continuous and the discrete model for the case of labyrinthic and spotted patterns.

diffusivity which in units of  $D_0$  is the function  $g$ , with two minima where particles will tend initially to clump (magenta vertical dashed lines in Fig. 8). As time advances a two-peak distribution establishes, which is the one-dimensional analogue of the two-dimensional rings observed before. This double peak, of a spatial size close to  $R_s$ , persists for extremely long times. However the inset in the bottom panel of Fig 8 shows that the diffusion coefficient in between the two peaks takes a nearly constant value which is very small but not zero ( $g(x) = D(x)/D_0 \approx 4 \times 10^{-6}$ ). This implies that at still longer times (of the order of  $R_s^2/D \approx 4 \times 10^5$  after the time displayed in the bottom panel of Fig 8) particles will diffuse between the two peaks, replacing them by a homogeneous distribution. The same will occur in two dimensions, since as showed in Fig. 9, the diffusion coefficient in the two-dimensional system is also homogeneous (but very small) inside the clusters so that at extremely long times the pattern of hollow clusters of Fig. 3 will be replaced by homogeneous clusters. Thus the ring structures seem to be a very-long lived transient state. They will disappear faster if the prescription in Eq. (3) for  $g$  is changed by another functional form with higher minimum values. Alternatively, for a choice such that  $g(x)$  is strictly zero for  $\tilde{\rho}_s \gg \tilde{\rho}_l$  then the rings will persist for infinite time as stationary structures.

## Discussion

We have studied how the combination of a short-range inhibition and a long-range activation in individual dispersal may influence the long-time spatial distribution of a population, which ranges from homogeneous to labyrinth and spot patterns depending on the relative weights of each mechanism. This type of behavior has been observed in mussel beds [32, 34, 35] where individuals tend to clump at short distance as a defensive strategy while competition for resources acts at a larger scale.

Pattern formation arises as a consequence of the interplay between inhibition and activation acting at different spatial scales that makes the spatially homogeneous state lose its stability. Resulting patterns show not only an inhomogeneous distribution of the population at a system level but also a not uniform distribution of the individuals within each cluster. For the time scales discussed here ring-like structures are formed, with most of the particles at the borders of the groups. This point has been studied from a simplified 1D situation starting from an initial density given by a step function. In the limits of this profile there are two regions where the nonlocal short and long-range densities are higher than the other, leading to the formation of annular structures. This mechanism will act for any kind of initial condition wherever there is a region where eventually the density is higher than in the rest of the system. Whether the rings will homogenize at very long times or rather they will remain stable depends on the details of the small-diffusion part of the

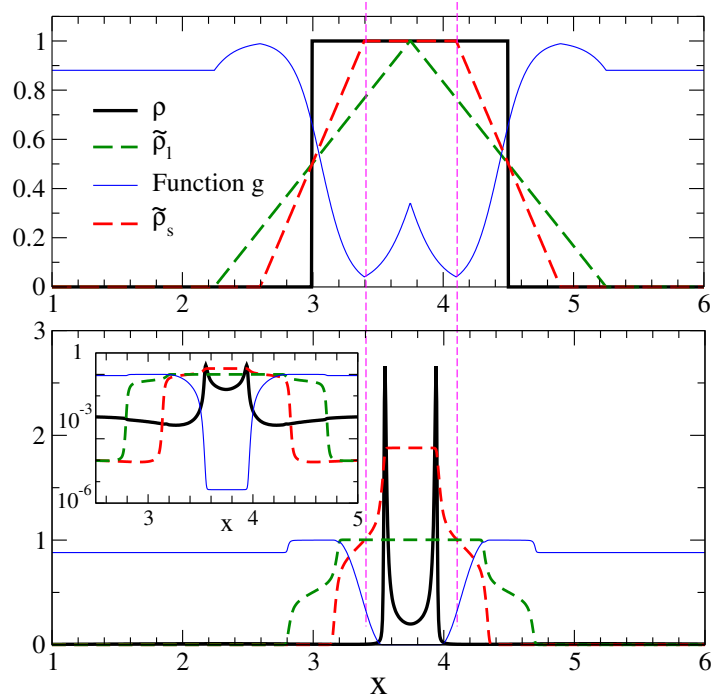


**Figure 8. Formation of ring-like structures in the 1D model.** Evolution of the 1D version of the model starting from an initial condition for  $\rho(x, t = 0)$  consisting on a pulse of height unity and length  $2R_l$  (displayed in the upper panel). The legend indicates the quantity represented by the different lines. The two vertical lines indicate the minima of the function  $g(x)$  (i.e. the diffusion coefficient in units of  $D_0$ ) at  $t = 0$  where particles will initially tend to accumulate. The bottom panel represent the same quantities (although  $\rho(x, t)$  has been divided by a factor 5 to fit into the same scale as the other curves) after a very long integration time ( $t = 6 \times 10^5$ ). A double-peak structure has developed. The inset displays this long-time configuration in logarithmic scale, showing that  $g(x) \approx 4 \times 10^{-6}$  in the central region. Parameters:  $a = 1$ ,  $b = 3.33$ ,  $c = 2.67$ ,  $D_0 = 10^{-4}$ ,  $R_l = 0.75$ ,  $R_s = 0.4$ ,  $N = \int dx \rho(x, t = 0) = 1.5$

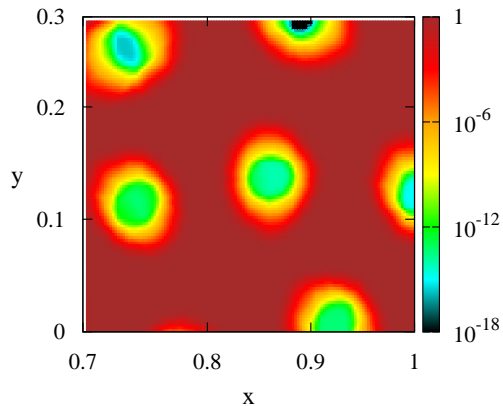


**Figure 9. Diffusion field in the 2D model.** Numerical computation of the function  $g$  as defined in Eq. (3) from the spot pattern showed in Fig. 3.  $g$  is extremely small inside the clusters, but not zero. Parameters:  $R_s = 0.05$ ,  $R_l = 0.1$ ,  $D_0 = 10^{-4}$ ,  $a = 1$ ,  $\rho_0 = 10^4$ ,  $b = 4.3 \times 10^{-4}$ ,  $c = 3.9 \times 10^{-4}$ . Zoom over the right lower corner of the pattern.

density-dependent diffusivity.

The particular shape of the structures depends on the relative importance of the short and long-range mean densities, weighted by the values of the parameters  $b$  and  $c$ . The first is the responsible of the formation of aggregates, so the model gives homogeneous distributions when this scale tends to zero ( $R_s \rightarrow 0$  or equivalently  $b = 0$ ). The larger one enhances the formation of groups. Individuals that do not belong to any group are surrounded by low densities in their close neighborhoods, but still can be in very far-populated regions. In these cases their movement has a larger diffusivity, so longer displacements are possible, increasing the probability of finding a group in a shorter time. A combination of both, a short- and a long-range dependence mobility, is an optimal mechanism to promote the formation of groups. In addition, the long-range competition stabilizes the ring-like structures since it avoids the formation of highly packed groups in a small area.

The generality of the model, a nonlinear diffusion equation with two nonlocal interaction scales that enhance and inhibit animal mobility, allows its application to a wide variety of ecological situations with these two ingredients. Moreover, our mathematical scheme shows a sequence of patterns that has been previously reported in natural systems such as mussel beds [35]. We recover both structures both in a stochastic and a deterministic description of the problem, suggesting that they are a result of the interplay between the two types of interactions with fluctuations playing a secondary role. Remarkably, our results bear similarities with results on vegetation patterns and fairy circles in arid regions [39, 40, 43] which arise from very different mechanisms, but have in common with our case the presence of competitive and facilitative interactions. We hope that our studies help the development of new mathematical models and more precise understanding of those situations where spatial distributions similar to the ones presented here are observed.

## Acknowledgments

We acknowledge fruitful discussions with Prof. Daniel Walgraef.

## References

1. Krapivsky P, Redner S, Ben-Naim E. A kinetic view of statistical physics. Cambridge: Cambridge University Press; 2010.
2. Murray JD. Mathematical Biology I: An Introduction. Berlin: Springer; 2002.
3. Okubo A, Levin S. Diffusion and ecological problems: modern perspectives. Berlin: Springer; 2001.
4. Castellano C, Fortunato S, Loreto V. Statistical physics of social dynamics. Rev Mod Phys. 2009 May;81(2):591–646.
5. Levin SA. The problem of pattern and scale in ecology. Ecology. 1992;73(6):1943–1967.
6. Young WR, Roberts AJ, Stuhne G. Reproductive pair correlations and the clustering of organisms. Nature. 2001 Jul;412(6844):328–31.
7. Hernández-García E, López C. Clustering, advection, and patterns in a model of population dynamics with neighborhood-dependent rates. Physical review E, Statistical, nonlinear, and soft matter physics. 2004 Jan;70(1 Pt 2):016216.
8. Heinsalu E, Hernández-García E, López C. Spatial clustering of interacting bugs: Lévy flights versus Gaussian jumps. EPL (Europhysics Letters). 2010 Nov;92(4):40011.
9. Vicsek T, Zafeiris A. Collective motion. Physics Reports. 2012;517(3):71–140.
10. Couzin ID, Krause J, James R, Ruxton GD, Franks NR. Collective Memory and Spatial Sorting in Animal Groups. Journal of Theoretical Biology. 2002;218(1):1–11.
11. Bialek W, Cavagna A, Giardina I, Mora T, Silvestri E, Viale M, et al. Statistical mechanics for natural flocks of birds. Proceedings of the National Academy of Sciences of the United States of America. 2012 Mar;109(13):4786–91.
12. Ward AJW, Sumpter DJT, Couzin ID, Hart PJB, Krause J. Quorum decision-making facilitates information transfer in fish shoals. Proceedings of the National Academy of Sciences of the United States of America. 2008 May;105(19):6948–53.
13. Lopez U, Gautrais J, Couzin ID, Theraulaz G. From behavioural analyses to models of collective motion in fish schools. Interface focus. 2012 Dec;2(6):693–707.
14. Martínez-García R, Calabrese JM, Mueller T, Olson Ka, López C. Optimizing the Search for Resources by Sharing Information: Mongolian Gazelles as a Case Study. Physical Review Letters. 2013 Jun;110(24):248106.
15. Tarnita CE, Taubes CH, Nowak MA. Evolutionary construction by staying together and coming together. Journal of Theoretical Biology. 2013;320:10–22.
16. Krause J, Ruxton GD. Living in groups. Oxford: Oxford University Press; 2002.
17. Flierl G, Grünbaum D, Levins S, Olson D. From individuals to aggregations: the interplay between behavior and physics. Journal of Theoretical biology. 1999 Feb;196(4):397–454.
18. Viswanathan GM, Da Luz MG, Raposo EP, Stanley HE. The physics of foraging: an introduction to random searches and biological encounters. Cambridge: Cambridge University Press; 2011.
19. Marchetti M, Joanny J, Ramaswamy S, Liverpool T, Prost J, Rao M, et al. Hydrodynamics of soft active matter. Reviews of Modern Physics. 2013;85(3):1143–1189.

20. Méndez V, Campos D, Bartumeus F. Stochastic foundations in movement ecology: Anomalous diffusion, front propagation and random searches. Berlin: Springer; 2014.
21. Burger M, Haškovec J, Wolfram M. Individual based and mean-field modeling of direct aggregation. *Physica D: Nonlinear Phenomena*. 2012;260:145–158.
22. López C. Macroscopic description of particle systems with nonlocal density-dependent diffusivity. *Physical Review E*. 2006 Jul;74(1):012102.
23. Méndez V, Campos D, Pagonabarraga I, Fedotov S. Density-dependent dispersal and population aggregation patterns. *Journal of Theoretical Biology*. 2012 Sep;309:113–20.
24. Raghil M, Levin SA, Kevrekidis IG. Multiscale analysis of collective motion and decision-making in swarms: an advection-diffusion equation with memory approach. *Journal of Theoretical Biology*. 2010 Jun;264(3):893–913.
25. Schellinck J, White T. A review of attraction and repulsion models of aggregation: Methods, findings and a discussion of model validation. *Ecological Modelling*. 2011 Jun;222(11):1897–1911.
26. Lefever R, Lejeune O. On the origin of tiger bush. *Bulletin of Mathematical Biology*. 1997;59(2):263–294.
27. Borgogno F, D’Odorico P, Laio F, Ridolfi L. Mathematical models of vegetation pattern formation in ecohydrology. *Reviews of Geophysics*. 2009;47(1):RG1005.
28. Martínez-García R, Calabrese JM, López C. Spatial patterns in mesic savannas: The local facilitation limit and the role of demographic stochasticity. *Journal of Theoretical Biology*. 2013;333(0):156–165.
29. Rietkerk M, Boerlijst MC, van Langevelde F, HilleRisLambers R, van de Koppel J, Kumar L, et al. Self-organization of vegetation in arid ecosystems. *The American Naturalist*. 2002;160(4):524–530.
30. Bonachela JA, Pringle RM, Sheffer E, Coverdale TC, Guyton JA, Caylor KK, et al. Termite mounds can increase the robustness of dryland ecosystems to climatic change. *Science*. 2015;347(6222):651–655.
31. Martínez-García R, Calabrese JM, Hernández-García E, López C. Minimal mechanisms for vegetation patterns in semiarid regions. *Philosophical Transactions of the Royal Society of London A*. 2014;372(2027):20140068.
32. van de Koppel J, Rietkerk M, Dankers N, Herman PMJ. Scale-dependent feedback and regular spatial patterns in young mussel beds. *The American Naturalist*. 2005 Mar;165(3):E66–E77.
33. Liu QX, Doelman A, Rottschäfer V, de Jager M, Herman PMJ, Rietkerk M, et al. Phase separation explains a new class of self-organized spatial patterns in ecological systems. *Proceedings of the National Academy of Sciences of the United States of America*. 2013 Jul;110(29):11905–11910.
34. van de Koppel J, Gascoigne JC, Theraulaz G, Rietkerk M, Mooij WM, Herman PMJ. Experimental evidence for spatial self-organization and its emergent effects in mussel bed ecosystems. *Science*. 2008 Oct;322(5902):739–742.
35. de Jager M, Weissing FJ, Herman PMJ, Nolet Ba, van de Koppel J. Lévy walks evolve through interaction between movement and environmental complexity. *Science*. 2011 Jun;332(6037):1551–1553.

36. Liu QX, Weerman EJ, Herman PMJ, Olff H, van de Koppel J. Alternative mechanisms alter the emergent properties of self-organization in mussel beds. *Proceedings of the Royal Society of London B: Biological Sciences*. 2012;279(1739):2744–2753.
37. Liu QX, Herman PM, Mooij WM, Huisman J, Scheffer M, Olff H, et al. Pattern formation at multiple spatial scales drives the resilience of mussel bed ecosystems. *Nature Communications*. 2014;5:5234.
38. Dean DS. Langevin equation for the density of a system of interacting Langevin processes. *Journal of Physics A: Mathematical and General*. 1996;29(24):L613.
39. Fernandez-Oto C, Tlidi M, Escaff D, Clerc M. Strong interaction between plants induces circular barren patches: fairy circles. *Philosophical Transactions of the Royal Society A: Mathematical, Physical and Engineering Sciences*. 2014;372(2027):20140009.
40. Sheffer E, Yizhaq H, Shachak M, Meron E. Mechanisms of vegetation-ring formation in water-limited systems. *Journal of Theoretical Biology*. 2011 Mar;273(1):138–146.
41. Pigolotti S, López C, Hernández-García E. Species clustering in competitive Lotka-Volterra models. *Physical Review Letters*. 2007;98(25):258101.
42. Martínez-García R, Calabrese JM, Hernández-García E, López C. Vegetation pattern formation in semiarid systems without facilitative mechanisms. *Geophysical Research Letters*. 2013;40(23):6143–6147.
43. Juergens N. The biological underpinnings of Namib Desert fairy circles. *Science*. 2013;339(6127):1618–1621.